Department of Environment Systems

Graduate School of Frontier Sciences

The University of Tokyo

2021

Master's Thesis

Effect of carboxylic acid modification on ZrO$_2$ nanoparticles synthesis in supercritical water

(カルボン酸による超臨界水中の表面修飾がジルコニウム酸化物微粒子合成に与える影響)

Submitted January 20, 2022

Adviser:　　Assistant Professor Akizuki Makoto

李雪

Li XUE

Catalogue

Chapter 1 Introduction

1.1 Nanoparticles and Synthesis Methods

Researches about nanoparticles with a diameter of about 1 to 100 nm has been received extensive attention for many years. The unique and tunable size-dependent properties of nanometers make nanoparticles excellent and critical performance in many fields [1]. Particles with nano-scale can greatly increase the surface area to volume ratio, which is very helpful to increase reaction rate in many catalytic or other reaction. Nanotechnology is already playing an increasingly important role in our daily lives, especially as energy and chemical or other resource efficiency. Currently, as consumers increasingly demand performance and miniaturization of products such as self-cleaning coatings, more and more advanced nanomaterials are becoming commercialized and entering daily life, including health care products like sunscreens, electronic products like battery materials and sensors, catalysts in a variety of industries [2]. These functional properties of nanoparticles are related to their size distribution, crystal structure, composition, dispersibility, and appearance. Therefore, for development of nanotechnology, it is important not only to synthesize new nano-materials, but also to develop updated and greener synthesis methods, which means the enhancement of function, the improvement in size control and the reduction of resource consumption during the nanoparticles synthesis process.

The particle synthesis methods can be roughly divided into the pulverization of raw materials into particles and the precipitation of particles from precursors such as ions and molecules, as Figure 1.1 [3]. The synthesis of nanoparticles mainly adopts the latter method. This bottom-up approach can be further divided into gas-phase and liquid-phase methods. When the gas phase method is used, the reaction proceeds at high temperature, the crystallinity is high, and single nanometer (particles with a particle size of 10 nm or less) can be synthesized. When the liquid phase method is used, the maneuverability of shape and size is high due to the influence of the solvent, but the

crystallinity is low. The commonly used method for metal oxide nanoparticles synthesis is the hydrothermal synthesis method. In hydrothermal synthesis, hydrothermal reactions occur through the nucleation and growth stages. Hydrothermal reactions, which include hydrolysis and dehydration of metal ions, are represented by the following equation (1) and (2) [4].

$$M(NO_3)_x + xH_2O \longrightarrow M(OH)_x + xHNO_3 \tag{1}$$

$$M(OH)_x \longrightarrow MO_{\frac{x}{2}} + \frac{x}{2}H_2O \tag{2}$$
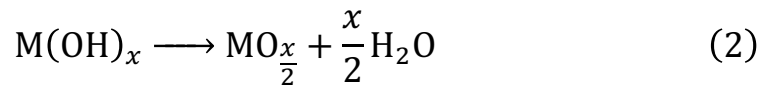
Temperature is one of most important parameters in hydrothermal synthesis. At different temperatures, the solubility of many metal ionic species have significant change, which is related to the particle size distribution [5]. Pressurization increases the water boiling point, allowing hydrothermal synthesis to be conducted at higher temperatures. Thus, controlling hot compressed water has been considered as a useful method to control the mental oxides nanoparticles synthesis.

1.2 Supercritical Hydrothermal Synthesis

The hydrothermal reaction equilibria of reactions shift to generate hydroxides and oxides as the temperature increases, particularly under supercritical conditions. Supercritical water refers to water above the critical point (374 °C, 22.1 MPa), with properties of water change dramatically. Figure 1.2 shows the temperature dependence of water properties at 25 MPa, such as density, viscosity, and dielectric constant. the density of supercritical water is lower than that of liquid water but is much higher than that of steam [6]. On the other hand, the viscosity of supercritical water is as low as that of steam [7]. Lower dielectric constant and solubility of ionic species lead to hydrothermal reactions with high reaction rates. Various studies on the supercritical hydrothermal synthesis method have been conducted in recent decades following the first proposal of the methodology [8].

With increased interest in both green and nanotechnologies, more sustainable manufacturing routes to crystalline inorganic nanomaterials are of interest [9, 10]. The vast majority of published literature on the syntheses of nanoparticles relates to materials prepared under static or batch processes or using multistep processes. More recently, an increasing number of publications have demonstrated the potential of rapid continuous methods for controlled manufacture of inorganic nanomaterials [11]. Among these reactions, the greenest and most promising can be considered those that are primarily water-based, that is continuous hydrothermal synthesis processes.

For the flow reactor, Reynolds number (*Re*) can be used to describe the mixing state. As the Reynolds number increasing, the mixture of inlet solution gets sufficient mixing. As shown in the Figure 1.3, Aoki *et al* described the particle size of the obtained CeO_2 nanoparticles at different temperatures and *Re* during mixing [12]. Flow rate and temperature increasing lead to *Re* increasing with an improvement in turbulence. In addition, the particle size became stable when the *Re* became much higher.

1.3 Modification

Not only the synthesis of nanoparticles, surface modification of those nanoparticles in the reaction during particle growth is also possible in supercritical water. As mentioned in last section, due to the low dielectric constant in supercritical water, the solubility of inorganic is extremely low. In contrast to ionic materials, nonpolar organic materials, which lead to phase separation in low temperature water, are miscible with supercritical water. This phase behavior is important for in situ organic surface modification. As shown in Figure 1.4, In situ organic modification process in supercritical water is like: (a) the binary system consists of organic phase and water phase with metal ions contained at room temperature; (b) a homogenous phase with metal oxides generation and organic modification at supercritical condition; (c) back to the binary system at room temperature and pressure, modified particles exist in organic phase [2]. In many cases, the organic modification are taken place in batch reactor. In

this study, the flow reactor would be used, and turbulence state in the reactor lead the system more homogenous.

Using in situ surface modification, particle size and shape control were achieved because the surfactant molecules can affect nucleation and growth. Fujii *et al.* reported that the amount of modification varies depending on the length of modifiers, resulting in particle size variation [13]. Taguchi *et al.* synthesized CeO_2 particles with cubic phase modified by lauric acid in supercritical water [14]. Surface modification makes an important role in nanomaterial synthesis because surface modified particles usually have smaller sizes, functional surface, and oriented structures [15].

1.4 Carboxylic Acid Modifier

The organic molecules with carboxyl group(-COOH) are generally used as the surface modifiers, which is also called carboxylic acid. Carboxylic acids with an aliphatic chain are attached to the surface of nanoparticles through coordination bond between the carboxylate anion (-COO$^-$) and metal cation, forming a monolayer films on particles. The tradition modification has major technological drawbacks including the slowness of process and the use of organic solvents [16]. With low polarity, supercritical water is considered as a green solvent for organics. The carboxylic acids are usually used as modifiers, such as acetic acid, hexanoic acid, lauric acid, but using dicarboxylic acid is actually less reported. Interestingly, Takami *et al*. found dicarboxylic acid combined two CeO_2 nanocrystals together. Dicarboxylic acid with two -COOH has the possibility to combine nanoparticles with both ends [17].

1.5 Zirconium Oxide

Zirconium oxide (ZrO_2) has been used widely as catalysts and ceramics due to its specific chemical and physical properties, such as high thermal stability, ionic conductivity, and oxygen storage capacity [18]. As Figure 1.5 shown, ZrO_2 has several crystalline phases, including amorphous, monoclinic, tetragonal and cubic phase,

leading to different functional performances. At ambient temperature and atmospheric pressure, ZrO_2 is usually stabilized in the monoclinic phase. Many applications of ZrO_2, such as thermal barrier coating, require tetragonal or cubic phases, which are normally produced from monoclinic phase through a reversible martensitic phase transformation at above 1200℃ [19].

ZrO_2 products are prepared commercially by precipitation or hydrolysis methods. For ZrO_2 nanoparticles, several ways have been developed for many years, like hydrothermal synthesis, sol-gel and combustion methods. In order to prepare more practical ZrO_2 nanoparticles, researchers focused on the control of size and phase. Hakuta et al. synthesized ZrO_2 particles with narrow size distribution of 5-8 nm in supercritical water of 400 °C, 30 MPa [20]. It has been known for some time that the tetragonal phase exists at room temperature in microcrystals. Garvie estimated the phases stability of nanocrystalline ZrO_2 and proposed the hypothesis that below the size with about 10 nm, ZrO_2 nanoparticles exist as stable tetragonal phases at room temperature [21]. Wu *et al*. modified the ZrO_2 nanoparticles surface by hexamethyldisilazane and they found the modified ZrO_2 nanoparticles increased the room temperature tetragonal phase stability [19]. Bokhimi *et al*. found acetic acid participated in the stabilization of tetragonal phase based on the C-O bonding [22]. It is attributed that the surface modification decreases interfacial energies and reduces the surface nucleation sites to control the grain growth. Thus, for ZrO_2 nanoparticles phase selectivity, getting small size and surface modification could be considered as important factors. Becker et al. prepared ZrO_2 with average size of 5-6 nm in sub- and supercritical water, of which all samples were the mixture of monoclinic and tetragonal ZrO_2 [23]. Taguchi et al. synthesized ZrO_2 nanoparticles with size of about 11 nm in presence of sebacic acid using supercritical batch reactor and found sebacic acid inhibited the growth of ZrO_2 due to surface modification [24].

1.6 Objective

This study aims to investigate the effect of various carboxylic acid modification on ZrO_2 nanoparticles which are synthesized in supercritical flow reactor. The specific objectives are:

∗   to explore the effect of modification on particles size and crystal phase;

∗   to measure the amount of modification and find the factors that influenced modification;

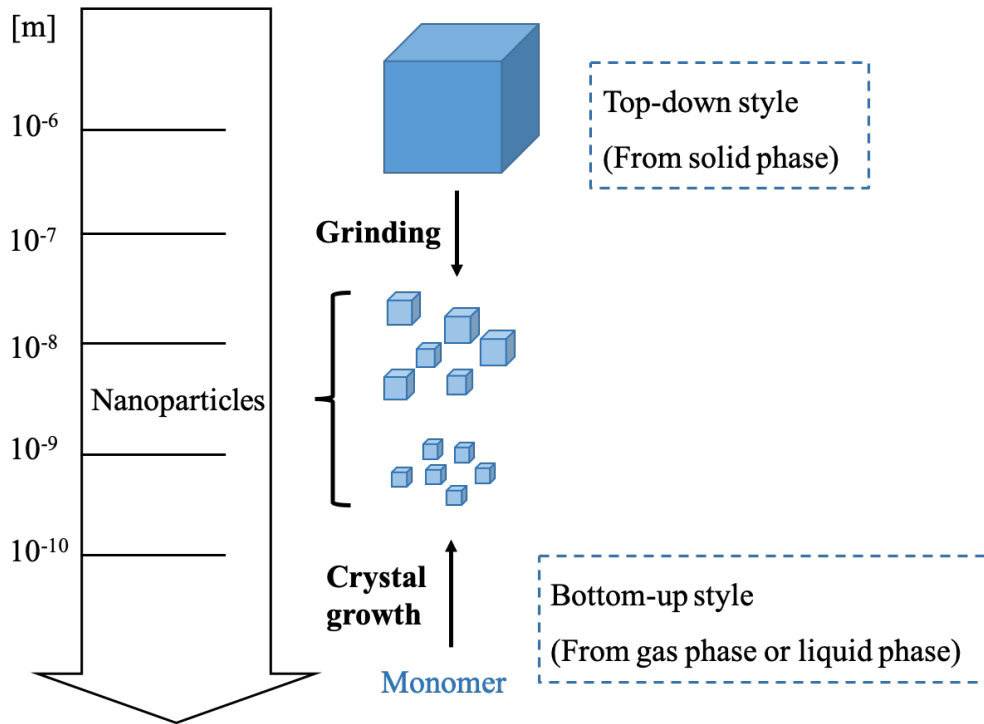∗   to explore the combination of mono- or di- carboxylic acids.
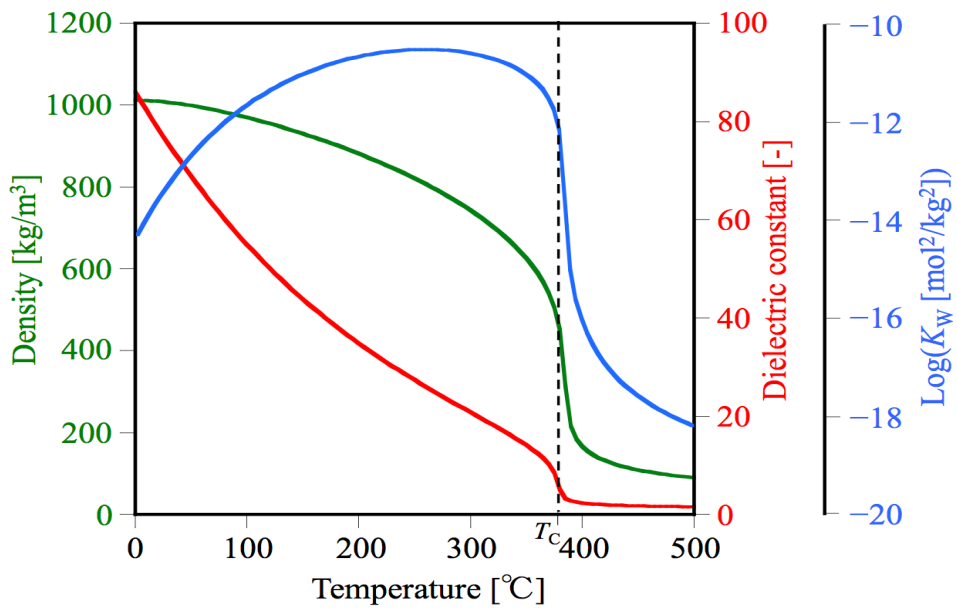
Figure 1.1 Particles synthesis methods

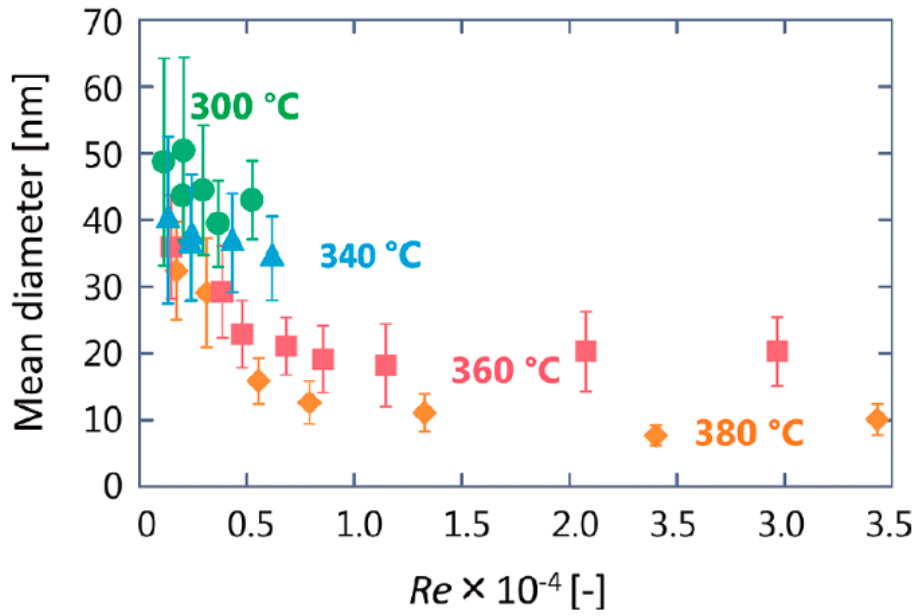**Figure 1.2 Properties of water at 25 MPa [25]**

Figure 1.3 Particle size of the obtained CeO₂ nanoparticles with different
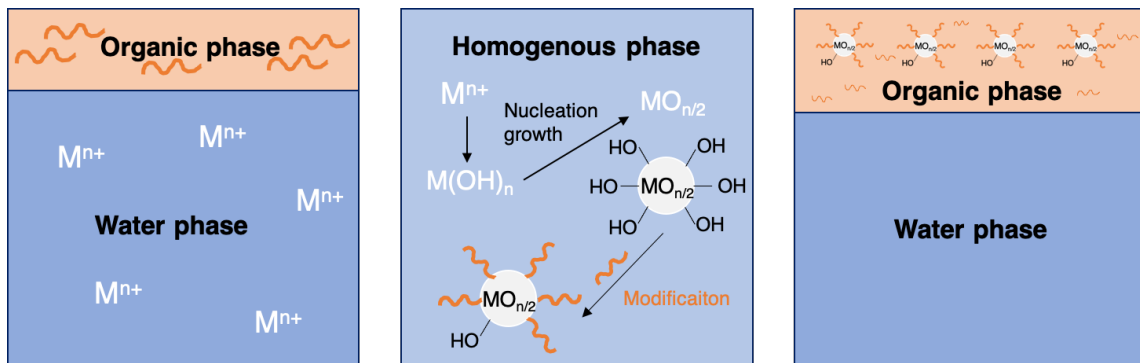
temperature and *Re* [12]

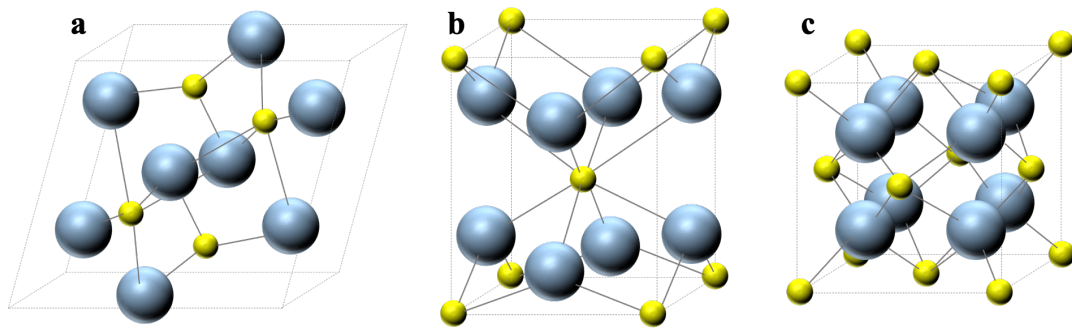**Figure 1.4 Process of in-situ organic modification in supercritical water**

Figure 1.5 Crystal structures of ZrO_2 with different phases (a) monoclinic; (b) tetragonal; (c) cubic

Chapter 2 Methodology

2.1 Materials

In the ZrO_2 nanoparticles synthesis experiment, used reagents, including the Zr precursor, carboxylic acids modifiers and solvent, are as following.

* $ZrO(NO_3)_2 \cdot 2H_2O$, Wako
* Distilled water, purified by AQUARIUS (made by RFD240HA, ADVANTEC))
* Ethanol (99.5%)   Wako
* HNO_3 Wako
* $CH_3(CH_2)_4COOH$ (Hexanoic Acid, HA)   Wako
* $HOOC(CH_2)_4COOH$ (Adipic acid, AA)   Wako
* $CH_3(CH_2)_8COOH$ (Decanoic acid, DA)   Wako
* $HOOC(CH_2)_8COOH$ (Sebacic acid, SA)   Wako

In the analysis experiment, the following reagents are used.

* CO_2 Standard Gas   JPF
* Air Standard Gas   Suzuki

2.2 Apparatus and Procedure

For ZrO_2 nanoparticles synthesis, the supercritical hydrothermal synthesis was performed in the supercritical continuous flow reactor. The apparatus is shown in Figure 2.1. The distilled water was heated by two electric furnaces in advance. Heated water, prepared Zr solution and modifiers solution were pumped into the reactor with ratio of 8:1:1. The distilled water was divided to two part, with each part of flow rate is 40 g/min. The flow rate of Zr solution and modifiers solution are both 10 g/min. Thus the total flow rate is 100 g/min. The Zr solution and modifier solution mixed first and then mixed with heated water rapidly at the mixer. In order to prevent the backflow caused by high temperature steam, the cooler was set before the mixer. The mixture of

feed solution entered the main reactor tube at about 400 °C and 30 MPa, for the residence time of 10 s. The pressure was adjusting by the back pressure valve (BP66-112865, Go Inc) setting at outfall. The temperature and pressure in each reaction section were output to a data logger (SMARTDAC + GM, Yokogawa) and monitored. The ZrO_2 nucleated and grow into nanoparticles with modification in the main reactor tube. The detail of the reactor will be introduced next. The metal salt products were cooled to suspension by cooler and collected in jar. These products suspension was subjected to the pressure filtration with nitrogen gas using a piece of nitrocellulose filter (Merck Millipore, VSWPI14250, diameter 142 nm, pore size 0.1 μm). After filtration, the nitrocellulose filter was transferred to the vacuum oven (Yamato, ADP-31) with the oil rotary vacuum pump (ST-50), dried for 24 hours. The products were collected from the dried filter membrane.

In the experiment process, before turning on the feeding pump, the faucets of cooling water were opened. At first, all pump enter water and the working condition of each pump need to be checked. The pressure of inside the reactor is adjusted to 30 MPa by manipulating the back pressure valve. After the leak check and the flow rate check, the ovens were turned on and temperature was set to 600 °C at first. When the temperature monitoring of the mixed solvent before the internal cooling water increased to 400 ℃, switched two 10 g/min inlets from water to Zr solution and modifiers solution. When the effluent started to get turbid, the effluent could be collected after about 5 min. And about 4000 mL suspension were collected, before stopping the furnaces. Keep water inlet until completely cooling the whole equipment. Finally nitrate acid solution at about 1 mol/L will be fed into the reactor to wash it after the reactor is cooled down to blow 100 °C.

2.3 Reactor Details

For the reactor design, there is reactor happened parts of the device that are closely related to the ZrO_2 nanoparticles synthesis in this study. Other parts are similar to the

ordinary supercritical continuous synthesis device, and have little influence on the experiment. Theses reactor happened parts are mixer, unions and tubes, shown as Figure 2.2 and Figure 2.3. The specific parameter of tubes and unions are shown as Table 2.1. The residence time and Reynolds number of each reactor parts are also calculated through following equations, shown in Table 2.1.

Residence time is

$$\tau = \frac{V}{Q/\rho_{\substack{400°C \\ 30\,MPa}}} = \frac{\pi \frac{d^2}{4} l}{Q/\rho_{\substack{400°C \\ 30\,MPa}}}$$

Reynolds number is

$$Re = \frac{dv\rho_c}{\mu} = \frac{d(\dfrac{Q}{\rho_{\substack{400°C \\ 30\,MPa}} \pi \frac{d^2}{4}})\rho_c}{\mu}$$

$\rho_{\substack{400°C \\ 30\,MPa}}$: Water density in supercritical condition of 400 °C and 30 MPa

Q : Mass flow rate

μ : Water viscosity

d : Tube inner diameter

l : Tube length

v : Flow velocity

When Reynolds number increased, the synthesized particles size and ranges of size both became small. Especially, after reaching turbulence state (Re>4000), the particle size decreases dramatically [12]. The small particles synthesis required the turbulence state. The tube 4 is the main reactor tube and has the longest residence time and lowest Reynolds number. At the reaction condition of 400 °C and 30 MPa, the water density and viscosity decreased to 357.43 kg/m^3 and 4.39×10^{-5} Pa・s, respectively. According to these parameters, in order to keep main tube 2 at turbulence state, the 1/2-inch steel

tube with inner diameter of 9.4 mm is chosen with Reynolds number of 5138. The residence time is 9.90 s in tube 4 and 10.01s in total. The residence time of other parts could be negligible, which is just 1% of the total.

2.4 Experiment Design

Since this study is to explore the carboxylic acid modification on ZrO_2 nanoparticles, the only variable is the modifiers. Zr precursor feed concentration was fixed at 0.002 mol/L. Temperature, pressure and flow rate also wouldn't be changed. In this study, there were 10 samples of ZrO_2 nanoparticles generated without or with various carboxylic acids modification. Table 2.2 shows the feed modifiers situation and other experiment condition. Ethanol was used as the co-solvent because the long alkyl chain acids, SA and DA, have the low solubility in water. Thus, in order to run the flow reactor, 5% vol ethanol was added to the feed solution. And to know the implication of ethanol, 5% vol only and 5% vol ethanol+0.02 mol/L AA as the modifiers solution were also performed.

2.5 Characterization

The collected ZrO_2 particles morphology were analyzed by XRD, TEM. The organic modification situation was analyzed by TG-DTA, FTIR, GC-TCD. The following describes each analysis.

2.5.1 XRD

For the produced particles, the crystal phase was identified and the crystallite size was evaluated by X-ray diffraction (Rigaku, SmartLab). The basic measurement conditions are scanning speed: 4 degree/min, slit: 2/3, and running range: 10-90 degree. The X-ray source is a line. From the obtained XRD pattern, the crystal structure was identified and the crystallite size was calculated. The Scherrer equation is expressed as follow.

$$\tau = \frac{K\lambda}{\beta cos\theta}$$

τ: Crystal size

K: Dimensionless shape factor

λ: X-ray wavelength

β: Line broadening at half the maximum intensity

θ: Bragg angle

In this study, the Jade6.0 software was used to do the full graph peak fitting and calculate the mean crystal size.

2.5.2 TEM

Transmission electron microscopy (TEM) is a popular technique used to disclose nano-materials, including size distribution, structure and so on. Before observation by using the transmission electron microscope (JEOL-2100, manufactured by JEOL Ltd), the nanoparticle samples were pretreated. For the pretreatment, first, collected and dried samples are ground into powder. Then a very small amount of powder sample was added to about 10 mL ethanol, and the particles were well dispersed in an ultrasonic water bath for 1 min. A drop of the treated dispersion sample was dropped on the copper microgrid (Cu 200 mesh, JEOL) placed on the filter paper and dried. Then the TEM can be observed. More than 10 photos were taken for each sample, and more than 100 nanoparticles were counted using ImageJ software to obtain the size distribution of nanoparticles.

2.5.3 TG-DTA

Thermogravimetric analysis was performed at a temperature range from room temperature to 800 °C at a heating rate of 10 °C/min under air and Ar atmosphere of 150 mmHg using a thermal analyzer (Thermo plus EV02 TG 8121; Rigaku Crop.). Though thermogravimetric analysis the amount of surface modifiers present on the nanoparticles can be estimated. The DTA component shows whether decomposition

processes are endothermic or exothermic. The DTA also measures temperatures corresponding to phase changes where no mass loss occurs, such as melting, crystallization and glass transitions.

2.5.4 FTIR

Fourier transform infrared (FTIR) spectra were recorded using a FT/IR-6600 (JASCO). The FTIR analysis method uses infrared light to scan test samples and observe chemical properties. The FTIR instrument sends infrared radiation of 4000 to 1000 cm^{-1} through the sample, with some radiation absorbed and some passed through. The absorbed radiation is converted into rotational and vibrational energy by the functional group on the samples. The resulting absorbed band at the detector presents as a spectrum at the range of 4000 cm^{-1} to 1000cm^{-1}. The powder sample mixed with KBr plate (Tablet Master, starter kit-05) to make the test sample by tableting.
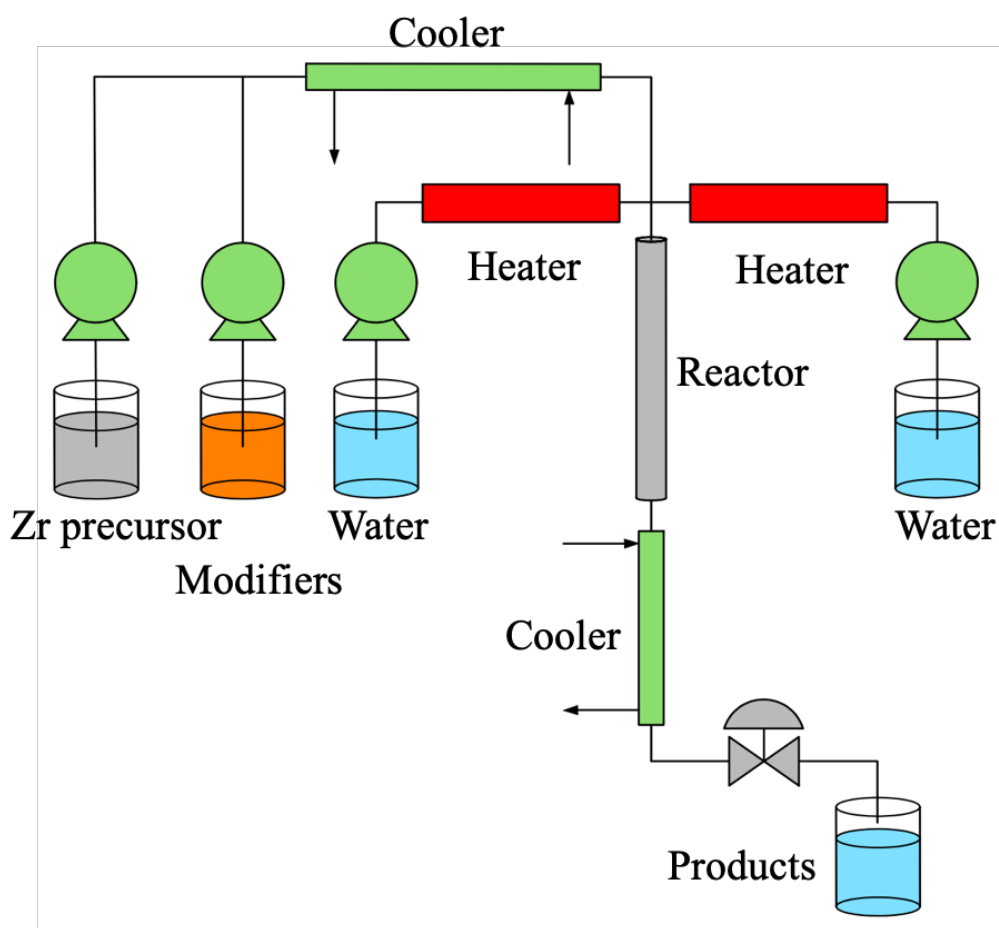
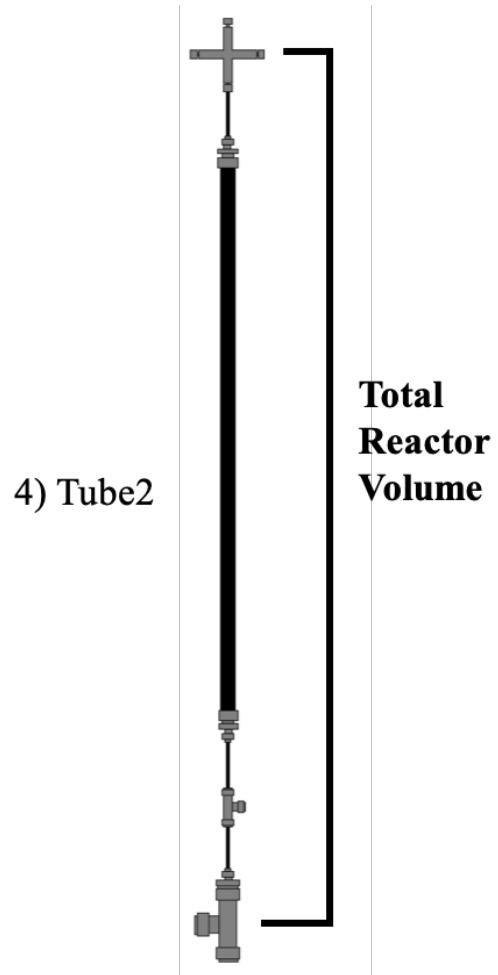**Figure 2.1 The apparatus of continuous supercritical flow reactor**
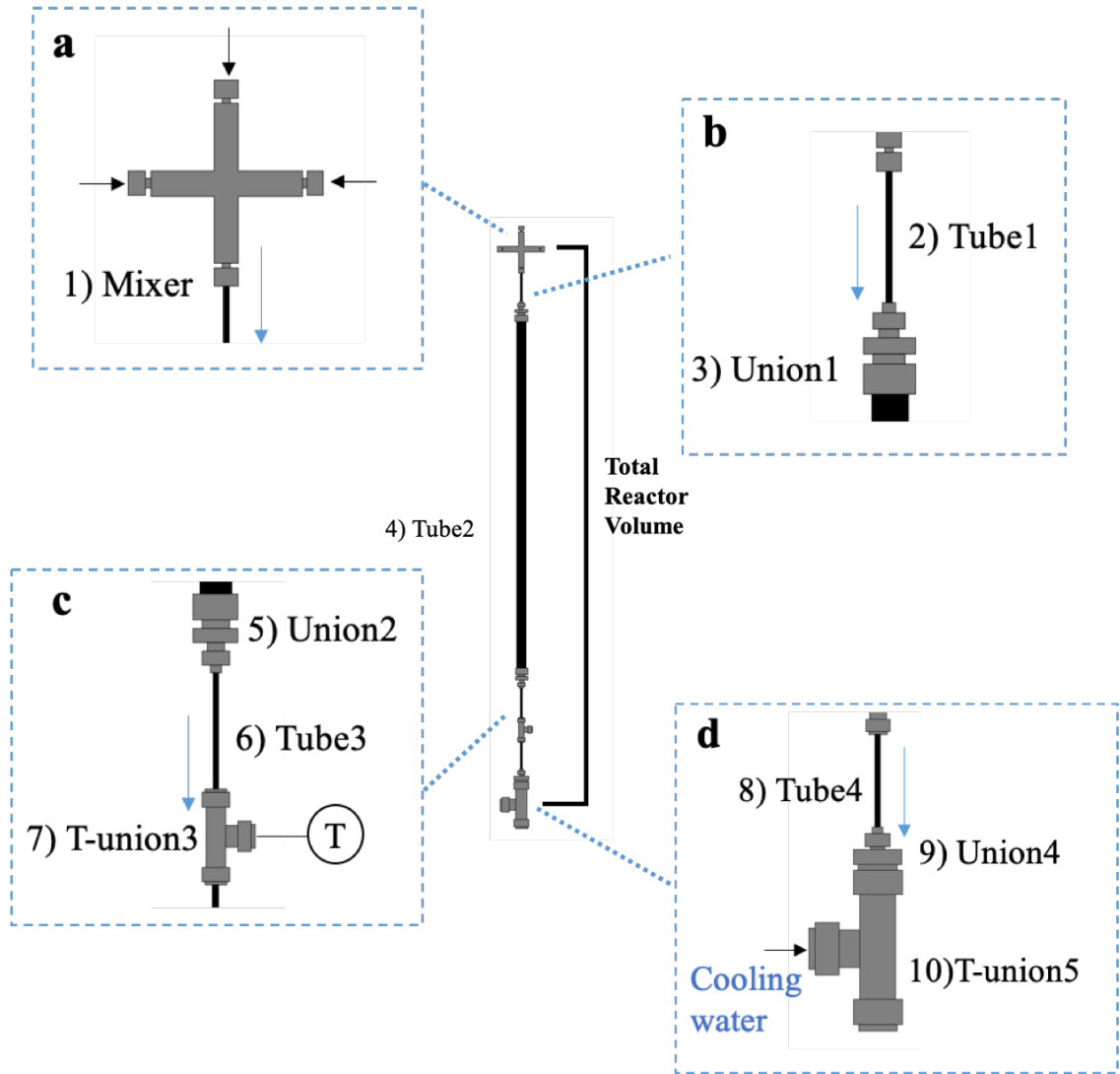
Figure 2.2 The main reactor details

a

1) Mixer

b

2) Tube1

3) Union1

4) Tube2

Total
Reactor
Volume

c

5) Union2

6) Tube3

7) T-union3

T

d

8) Tube4

9) Union4

10)T-union5

Cooling
water

Figure 2.3 The main reactor details

Table 2.1 The reactor unit parameters

Temperature	Pressure	Density	Viscosity	Flow rate
400℃	30 MPa	357.43 kg/m³	4.39×10^{-5} Pa·s	100 g/min

	(1) Mixer	(2) Tube1	(3) Union1	(4) Tube2	(5) Union2	(6) Tube3	(7) T-union3	(8) Tube4	(9) Union4	Total
Size (inch)	1/8	1/8	1/2-1/8	1/2	1/2-1/8	1/8	1/8	1/8	1/8-1/2	
Inner diameter (mm)	1.755	1.755	2.3	9.4	2.3	1.755	2.3	1.755	2.3	
Length (mm)	22.4	40	9.6	665	9.6	40	19.4	40	9.6	
Residence time (s)	0.0116	0.0208	0.0086	9.8971	0.0086	0.0208	0.0173	0.0206	0.0086	10.014
Re	27520	27520	20999	5138	20999	27520	20999	27520	20999	

Table 2.2 Experiment conditions

Sample Name		Distilled water flow rate	Zr precursor Concentration	Zr precursor Flow rate	Modifier Concentration	Modifier Flow rate	Experiment Condition Temperature	Experiment Condition Pressure
1	UM–ZrO$_2$				Distilled water			
2	002HA–ZrO$_2$				0.002 mol/L HA			
3	006HA–ZrO$_2$				0.006 mol/L HA			
4	002AA–ZrO$_2$				0.002 mol/L AA			
5	006AA–ZrO$_2$				0.006 mol/L AA			
6	E–ZrO$_2$				5% vol Ethanol			
7	002SA–ZrO$_2$	80 g/min	0.002 mol/L	10 g/min	0.002 mol/L SA +5% vol Ethanol	10 g/min	400 °C	30 MPa
8	006SA–ZrO$_2$				0.006 mol/L SA +5% vol Ethanol			
9	EAA–ZrO$_2$				0.002 mol/L AA +5% vol Ethanol			
10	DA–ZrO$_2$				0.002 mol/L DA +5% vol Ethanol			

Chapter 3 Results and Discussion

3.1 ZrO$_2$ Nanoparticles

In this section, the synthesis situation and in-situ organic modification of ZrO$_2$ nanoparticles were investigated. Table2.2 showed that there are 10 samples prepared in the preparation part. UM-ZrO$_2$ is the abbreviation of unmodified zirconia. About sample names, for example, "002"in 002HA-ZrO$_2$ means modifier concentration is 0.002 mol/L, and HA is the modifier species. Especially, in order to dissolve insoluble sebacic acid (SA) and Decanoic acid (DA), 5 % vol. ethanol was added to modifier solution. And EAA-ZrO$_2$ was prepared to explore the effect of ethanol, comparing with the sample 002AA-ZrO$_2$. To differentiate, "E", on behalf of ethanol, was added to form the E-ZrO$_2$ and EAA-ZrO$_2$. Although sebacic acid modified ZrO$_2$ and decanoic acid modified ZrO$_2$ were also synthesized in presence of 5 % vol. ethanol, for uniform formation of names, "E" was elided. In addition, using decanoic acid as modifiers, most of collected product was paste instead of powder like other products. According to TG results, the collected product is the mixture of minor Zirconia and major organics, like the residual of decanoic acid probably. Thus, in preparation experiment, the group of 0.006 mol/L DA was not conducted. These produced particles were analyzed by XRD, TEM. Then, the size and composition change of the composite oxide particles due to the presence of acid were compared, and the effect of in-situ organic modification on the composite process was discussed.

3.1.1 Appearance and crystal phase

The prepared products after drying for 24 h were transparent film shape on the filter paper. Figure 3.1 shows the appearance of 002AA-ZrO$_2$ products on the filter paper. Figure 3.2 shows the appearance of collected ZrO$_2$ products. Most of the ZrO$_2$ products are film-shape with little yellow. The E-ZrO$_2$ was extremely pure transparent. SA-ZrO$_2$ products were opacification, probably attributed to lots of surfaces modifiers. DA-ZrO$_2$

dried products was dark white paste shape as Figure 3.3, which is probably attributed to massive DA residual.

In order to verify the products are actually ZrO_2, XRD analysis was performed for each samples. For comparing easily, the XRD patterns of modifiers with feed concentration of 0.002 mol/L, was shown as Figure 3.4. The broad diffraction peaks in the XRD patterns indicate particles with small crystallite sizes. The particles size will be discussed in next section. The modified and unmodified ZrO_2 samples mainly show monoclinic phase, for peaks can be observed at 2θ values of 28.2° and 31.5°, corresponding to the monoclinic phase plane M (-111) and M (111). AA-ZrO_2, EAA-ZrO_2 and E-ZrO_2 show the shoulder peak at 2θ values of 30.1°. DA-ZrO_2 and SA-ZrO_2 show peak with strong intensity at the same place, which is corresponding to the tetragonal phase plane T (101). The carboxylic acid modification probably has an effect on crystal structures, oriented to generating tetragonal phases. The addition of ethanol has the effect on tetragonal phase formation, which is also reported in other researches [26]. Compared SA-ZrO_2 to EAA-ZrO_2, both with 5% vol ethanol, long chain carboxylic acid revealed stronger tetragonal peak in XRD patterns. The possible reason of effect on crystal phase is that when modifiers bind to the particles plane T (101), the growth rate of T (101) decreases, leading to tetragonal ZrO_2.

In addition, the feed concentration also exhibited some influence on the crystal phase. The 0.02 mol/L and 0.06 mol/L feed concentration of HA, AA, SA XRD patterns were compared in Figure 3.5 and Figure 3.6. 002HA-ZrO_2 almost have the same pattern with UM-ZrO_2, but 006HA-ZrO_2 showed a shoulder peak assigned to tetragonal phase at 30.1 °. In 002AA-ZrO_2 and 006AA-ZrO_2 patterns, there were both two peaks but when concentration increased, the peak at 31.5 ° shifted to 30.1 °. The difference between 002SA-ZrO_2 and 006SA-ZrO_2 patterns was more obvious. The tetragonal peak dominated in 006SA-ZrO_2 pattern, since the intensity of monoclinic peak was far below the intensity of tetragonal peak. In the 002SA-ZrO_2 pattern, the intensity of monoclinic and tetragonal were similar. If quantitative analysis of XRD patterns could be

performed, the accurate phase ratio would be calculated. Although these are the qualitative analysis through the patterns and intensity, but it still has reference values on that higher feed concentration of modifiers leads to more tetragonal ZrO_2 generated.

3.1.2 Morphology and size

The TEM images recorded the morphologies of ZrO_2 nanoparticles. The TEM images and size distributions of UM-ZrO_2 nanoparticles are shown in Figure 3.7. The TEM images of other samples are shown in Figure 3.8 and Figure 3.9. Regardless of modifier species or existence of ethanol, ZrO_2 nanoparticles has almost the same sizes and structure. According to TEM images, for all products, most of particles appeared like distorted spheres. And some particles appeared like polygon with sharp edges, which can be recognized as hexagon or octagon. Usually, ZrO_2 nanoparticles with monoclinic structure could be seen as hexagon. TEM results also show the ZrO_2 nanoparticles cluster into dense agglomerates with or without modification. Although the products color has changed with carboxylic acid modification as mentioned in former section, from TEM images, it is difficult to find the effect of carboxylic acid modification on the morphologies of ZrO_2 nanoparticles.

The particles size estimates were obtained from TEM images. Figure 3.7 shows the size distribution of UM-ZrO_2 and other samples' size distribution are shown in Table 3.1. The arithmetic mean size and distributions is obtained by counting more than 50 particles from more than ten TEM images for each ZrO_2 samples. Due to the incomplete and unclear defects of these TEM images, the data of size might still deviate from the real size distribution, but it can be trust relatively. As mentioned in 2.5.1 XRD section, crystalline size could be calculated through the Scherrer equation, which are also shown in Table3.1. Crystal size usually describes the crystallite, which can be mono-crystalline. Particles can be mono- or poly- crystalline or amorphous. Thus, particles size from TEM images is larger than crystal size from XRD patterns in many cases. In Table 3.1, crystal sizes calculated by XRD are 4.9~7.8 nm. From Table 3.1, mean sizes obtained

from TEM are 6.2~7.8 nm. Crystal sizes are a little bit smaller than particles sizes. It is possible that the most of nanoparticles observed in TEM images are monocrystalline, so that particle sizes are so close to crystal sizes. Interestingly, 006SA-ZrO$_2$ has the smallest particle size of 6.2 nm and crystal size of 4.9 nm. It indicated that long alkyl carboxylic acid with higher concentration has the possibility to generate more nanoparticles with small size but the differences with other samples is not large enough to improve the effect of SA modification on size control. Generally, most of modifiers seem to have little effect on size at such small scales, or possibly the modification is not sufficient.

3.2 Modification

In this section, the situation of carboxylic acid modification would be discussed. The situation means two questions. The first question is whether the modifiers were actually attached to ZrO$_2$ particles. And the second question is how and how much modifier did combine to ZrO$_2$ particles. The ZrO$_2$ products were detected by TG-DTA and FTIR.

3.2.1 TG-DTA

To quantitatively estimate the amount of modifiers attached to the surface of ZrO$_2$ nanoparticles, TG-DTA analysis have been performed. TG curves of all products are shown in the Figure 3.10 (a), (b). DTA curves of all products are shown in Figure 3.11. TG curves exhibited the mass loss and DTA curves revealed the exothermic and endothermic situation during the temperature rising process. At the range of 250-400°C, DTA curves of all modified ZrO$_2$ show the exothermic peak but no obvious peak appears on UM-ZrO$_2$ and E-ZrO$_2$ curves. Figure 3.10 shows that at same range of 250-400°C, all modified ZrO$_2$ have a distinct decrease on TG curves, exactly corresponding to peak position on DTA curves.

The exothermic peaks in DTA curves and distinct mass loss in TG curves are

attributed to modifiers combustion, which can be considered as the amount of modifiers. However, the UM-ZrO$_2$ and E-ZrO$_2$ also has continuously mass loss for chemisorbed water. For modified ZrO$_2$, the continuous mass loss without exothermic peak existed before and after modifier combustion. Thus, it is easier to consider that evaporation of chemisorbed water also happened with modifier combustion. The TG curves of UM-ZrO$_2$ actually could be divided to three parts depending on the curve shape. Below 100 ˚C, the mass loss caused by the evaporation of water increase rapidly. Between 100 to 500 ˚C, the mass loss was approaching linear. As temperature of above 500 ˚C, the mass loss almost stopped. So at range of 250-400˚C, the chemisorbed water loss in modified ZrO$_2$ was approached linear as well, probably. Based on this assumption, Figure 3.12 tells the calculation way of modifiers. Using origin software, draw two parallel lines tangent to the curves before and after distinct mass loss. Calculate the linear equations and the difference between the intercepts of the two lines is the amount of modification. The calculated amount of modifier is shown in Table 3.1. Also, the total mass loss and the weight ratio of modifier are calculated in Table 3.1.

The surface modifiers of AA-ZrO$_2$ are more than of HA-ZrO$_2$, which tells AA is probably easier to bind to ZrO$_2$ due to two -COOH. The SA molar amount of SA-ZrO$_2$ was twice than the AA molar amount of AA-ZrO$_2$. SA-ZrO$_2$ with different modifiers feed concentration show that higher concentration leading to more modifiers attached to particles. The modifier ratios of SA-ZrO$_2$ and EAA-ZrO$_2$ are larger, corresponding to less chemisorbed water loss. Nevertheless, DA-ZrO$_2$ shows not only exothermic peak but also the endothermic peak with approximately 50% mass loss from 100 to 200 ˚C, which is caused by the sublimation or evaporation of DA.

3.2.2 FTIR

The coordination bonds are assessed by FT-IR analysis as Figure 3.13. In the 1000-2000 cm^{-1} region, the pure AA, pure SA spectra and modified products have the peaks at 1408 cm^{-1} (v_s -COO$^-$), 1537 cm^{-1} (v_s -COO$^-$) and 1450 cm^{-1} (δ_{sc} -CH$_2$-), assigned to

the symmetric stretching mode of -COO⁻, the asymmetric stretching mode of -COO⁻, and scissoring bending mode of -CH_2- in the alkyl chain, respectively. In contrast, these absorbed bands do not appear on UM-ZrO_2 and E-ZrO_2 spectra, which do not exist organic acids. The pure acid AA and SA shows a strong band at 1700 cm⁻¹, which is assigned to the stretching mode of the free carboxyl group (-COOH). It indicates modifiers are attached to the surface of the modified ZrO_2 nanoparticles by the bidentate coordination bond of the carboxylate group (-COO⁻).

In the 2500-4000 cm⁻¹ region, SA-ZrO_2 spectrum also appears two absorbed peaks at 2920 (v_{as} -CH_2-), 2850 (v_s -CH_2-) cm⁻¹, assigned to the asymmetric stretching mode of -CH_2-, the symmetric stretching mode of -CH_2-, respectively. These bands of -CH_2- do not show on short chain acid AA and HA modified products, probably attributed to the long alkyl chain of SA. ZrO_2 products shows broad bands at 3400 cm⁻¹ and around1600 cm⁻¹, which can be assigned to the O-H modes of chemisorbed water and terminated hydroxides at the surface. The weak O-H absorbed band exist in SA-ZrO_2 and EAA-ZrO_2 spectra, agreed with the TG results, which tells less existence of chemisorbed water on SA-ZrO_2 and EAA-ZrO_2 particles.

In addition, compared with pure carboxylic acid with two -COOH, free -COOH are not observed in products modified by AA but observed in SA-ZrO_2 spectrum. It suggests probably more AA combined to ZrO_2 nanoparticles with both two carboxyl groups than SA. The length of alkyl chain has the possibility to influence the combination of dicarboxylic acids.

3.3 Mechanism of Carboxylic Acid Modification

In this section, the mechanism of carboxylic acid modification was discussed. The modified ZrO_2 nanoparticles showed tetragonal phases selectivity and decrease of chemisorbed water.

According to the critical size effect, which tells when nanoparticles' size below the critical size, tetragonal phases would be dominate. In this study, the particles size barely

changed with organic modification, but the tetragonal phase ratio increased. So the size effect theory is probably not the reason of tetragonal phase selectivity in this experiment. There are other theories considered with crystal phase. Generally, low pH enable stabilization of monoclinic ZrO_2, high pH conditions (pH > 9) favor the formation and stabilization of tetragonal ZrO_2. SA with long alkyl chain performs less acidity than AA. But the 0.006SA should be more acidic than 0.002SA, and 006SA-ZrO_2 has higher selectivity of tetragonal phase. As mentioned before, the existences of chemisorbed water and hydroxyl (O-H) on surface of EAA-ZrO_2 and SA-ZrO_2 particles are less than other products. At the same, the performance on tetragonal-orientation of SA-ZrO_2 and EAA-ZrO_2 are better than other products. There might be a correlation between chemisorbed water and phase selectivity.

On the other hand, ethanol also take a important role in supercritical fluids technology, the influence of ethanol could not be ignored. Compared with UM-ZrO_2, E-ZrO_2 also existed tetragonal peak as a shoulder peak and less mass loss from TG curves. If the total mass loss was considered as total chemisorbed water, then E-ZrO_2 contained less water. These explanations just the deduction from some results, which still need further research.

3.4 Summary

This chapter mainly discussed the results of ZrO_2 nanoparticles synthesis with various carboxylic acid modification. The results are divided to two parts, one of which is morphologies and another is modification situation. The mechanism of carboxylic acid modification parts still need further study.

Figure 3.1 The picture of 002AA-ZrO₂ sample
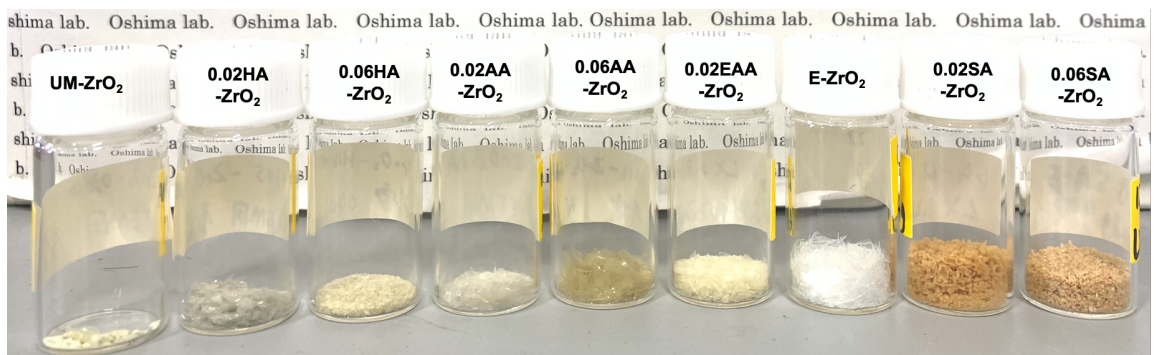
Figure 3.2 The appearance of ZrO₂ products
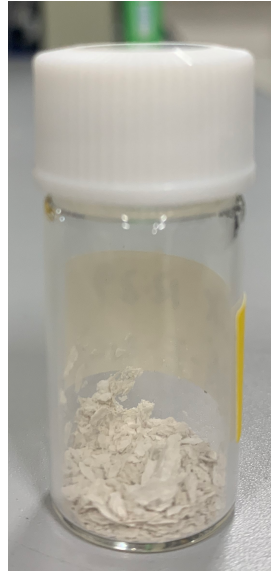
Figure 3.3 The appearance of DA-ZrO₂ products
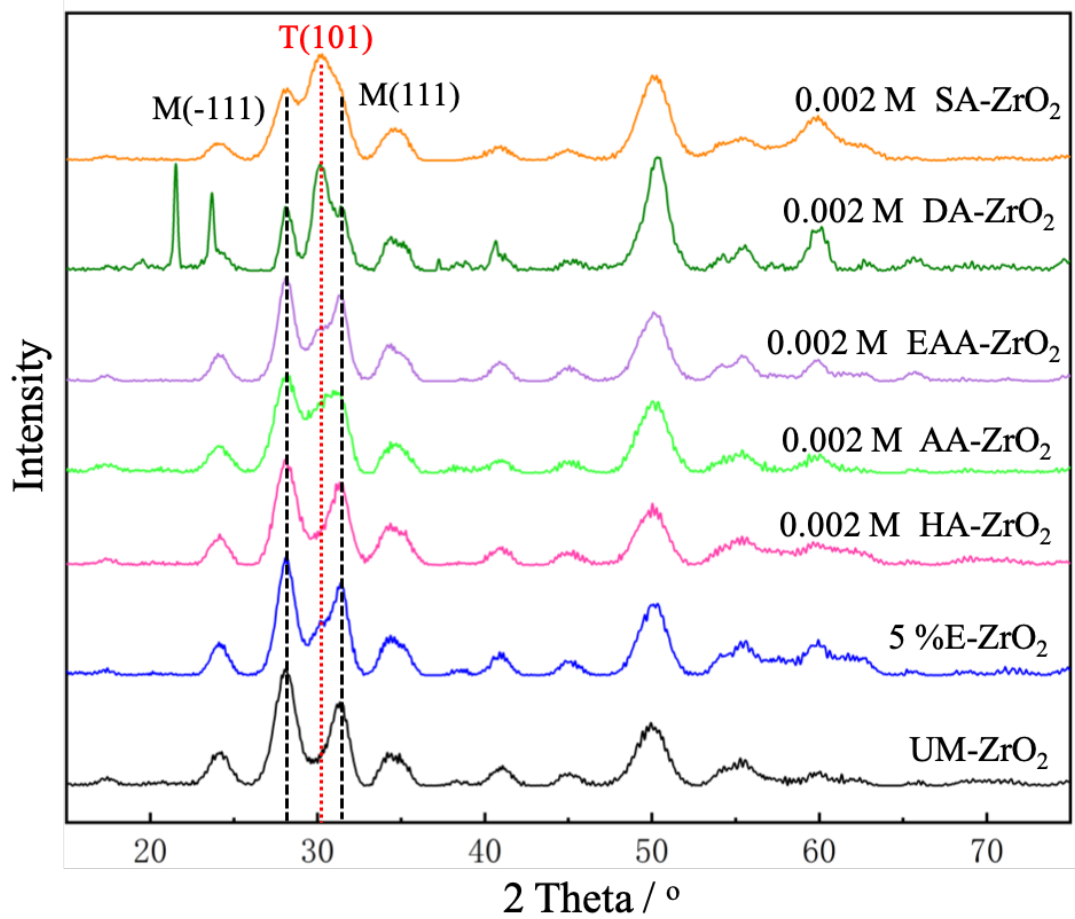
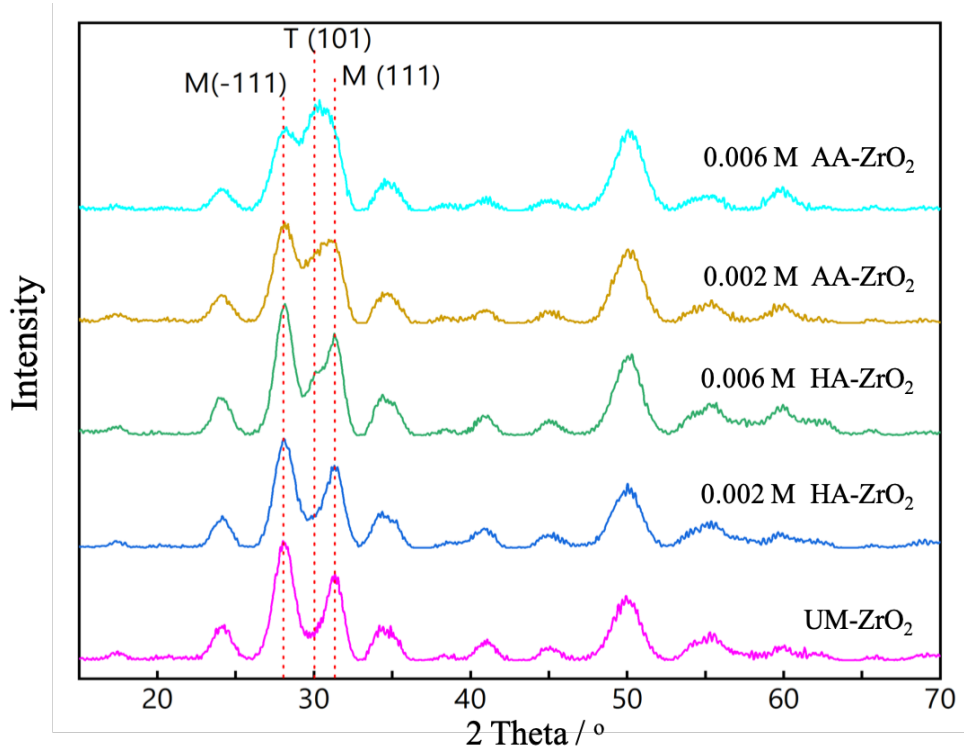**Figure 3.4 The XRD patterns (concentration of modifiers is 0.002 mol/L)**

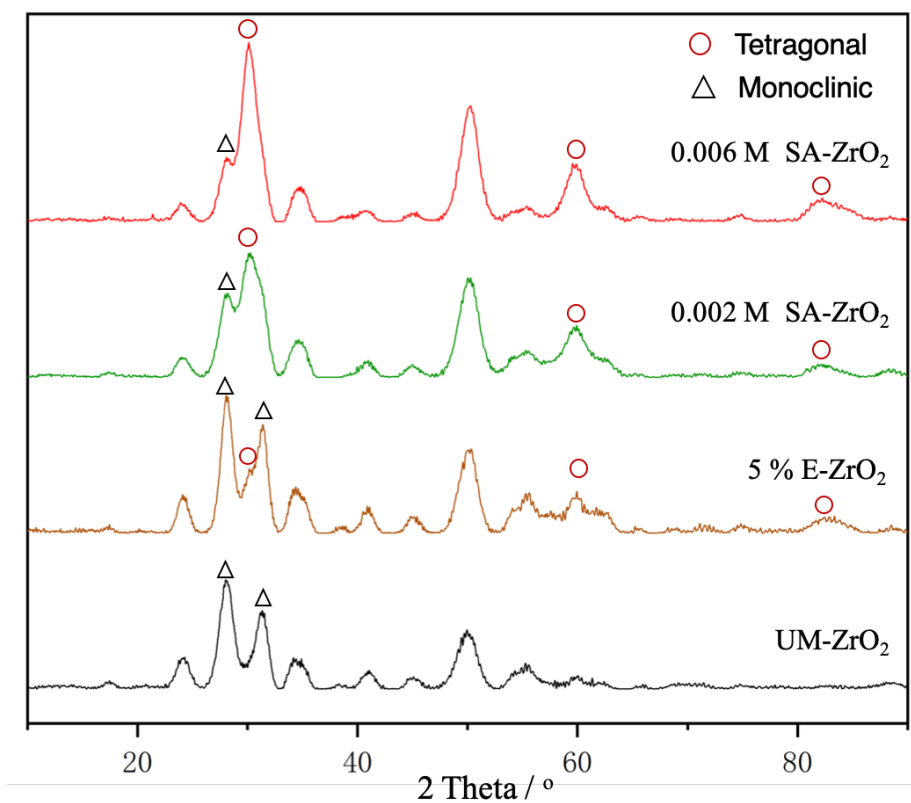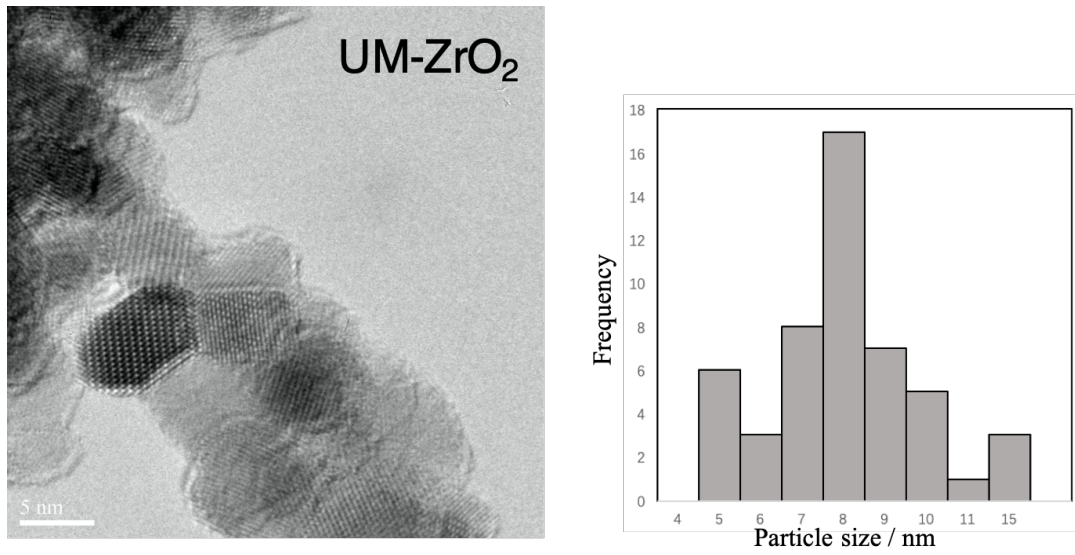**Figure 3.5 The XRD patterns**

Figure 3.6 The XRD patterns

Figure 3.7 TEM images and particles size distributions of UM-ZrO₂

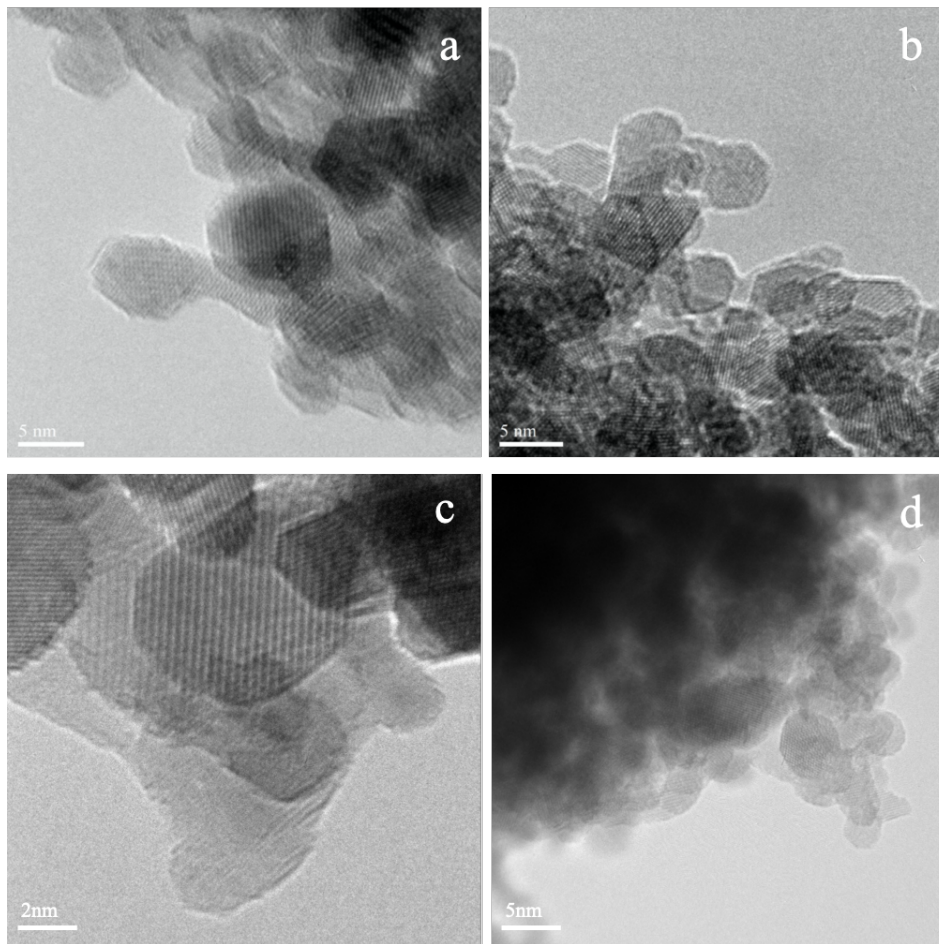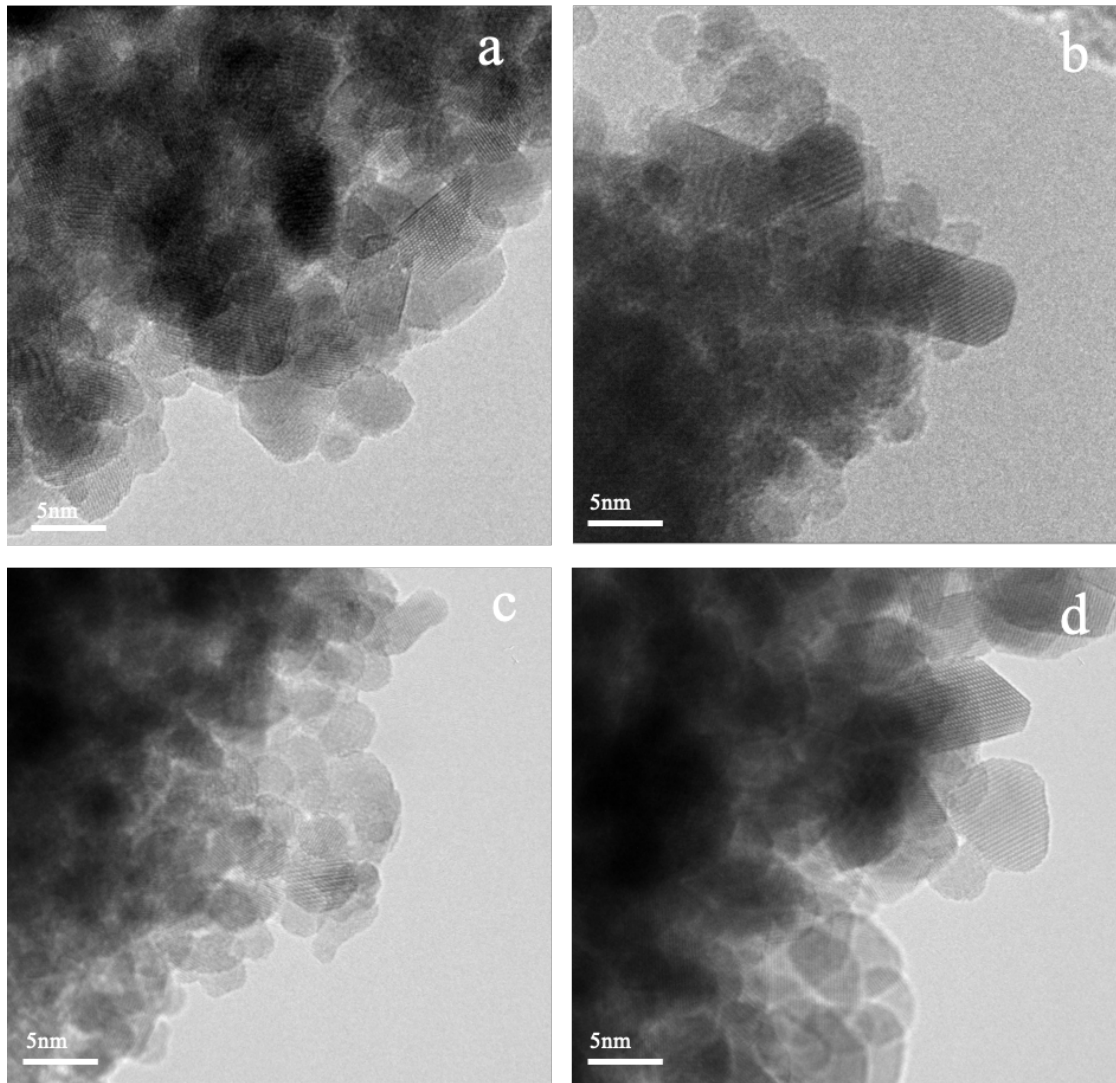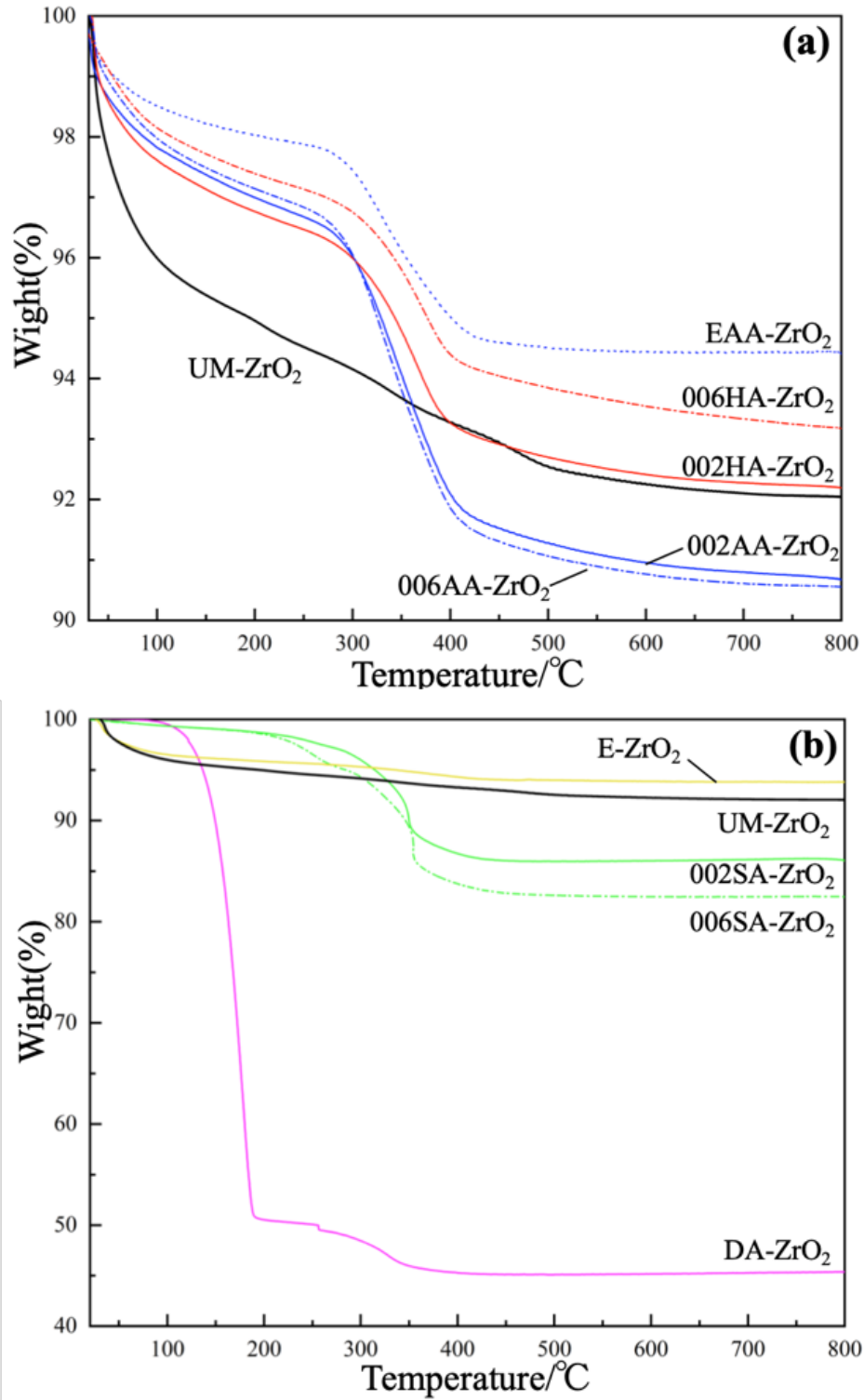**Figure 3.8 TEM images and particles size distributions of (a) 002HA-ZrO₂; (b) 002AA-ZrO₂; (c) 006HA-ZrO₂; (d) 006AA-ZrO₂**

Figure 3.9 TEM images and particles size distributions of (a) E-ZrO$_2$; (b) 002SA-ZrO$_2$; (c) 006SA-ZrO$_2$; (d) EAA-ZrO$_2$

Figure 3.10 TG Curves of (a) UM-ZrO$_2$, 002HA-ZrO$_2$, 002AA-ZrO$_2$, 006HA-ZrO$_2$, 006AA-ZrO$_2$, EAA-ZrO$_2$;

(b) UM-ZrO$_2$, E-ZrO$_2$, 002SA-ZrO$_2$, 006SA-ZrO$_2$, DA-ZrO$_2$
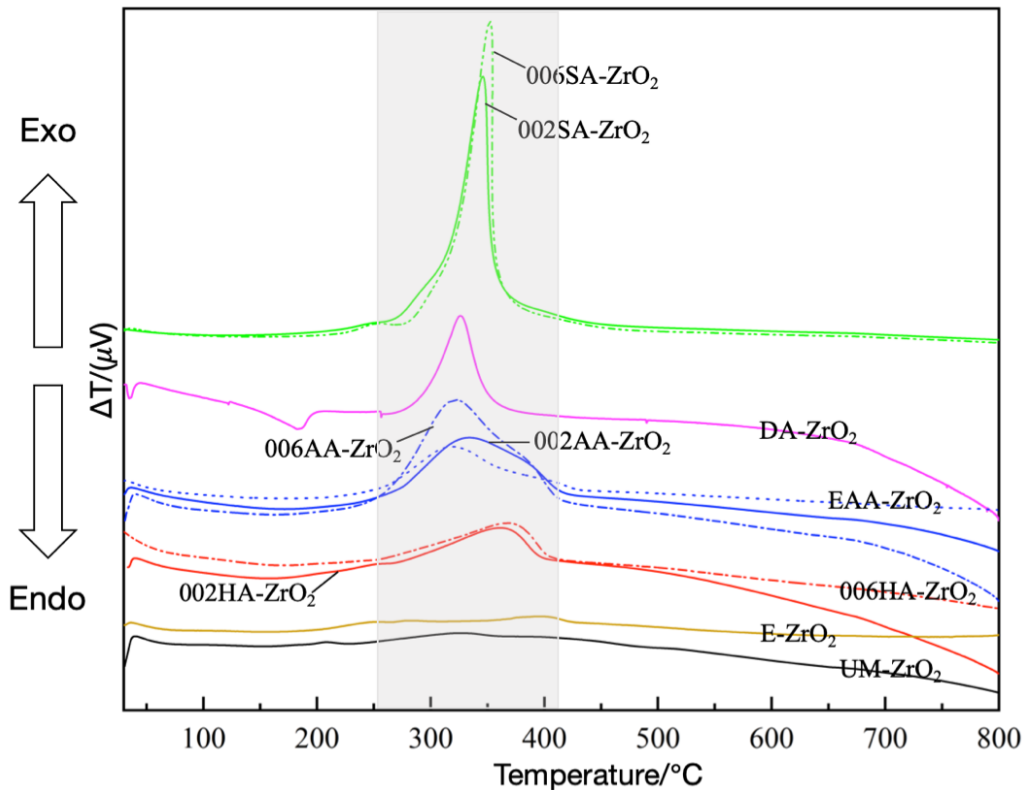
Figure 3.11 DTA Curves of all samples
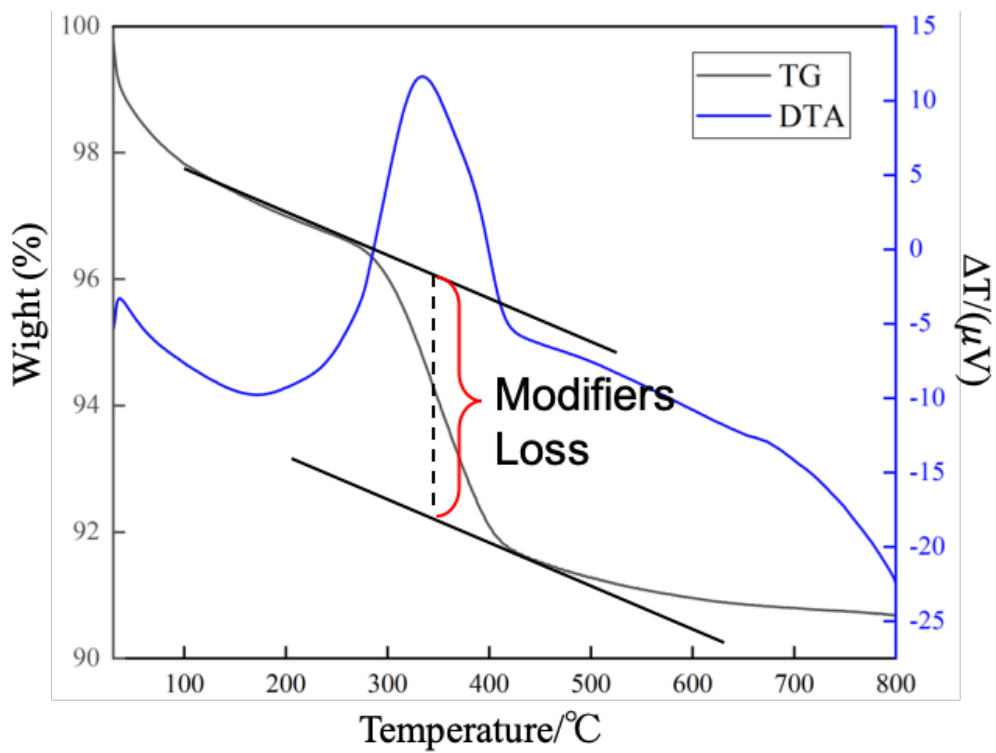
Figure 3.12 TG-DTA Curves of 002AA-ZrO$_2$
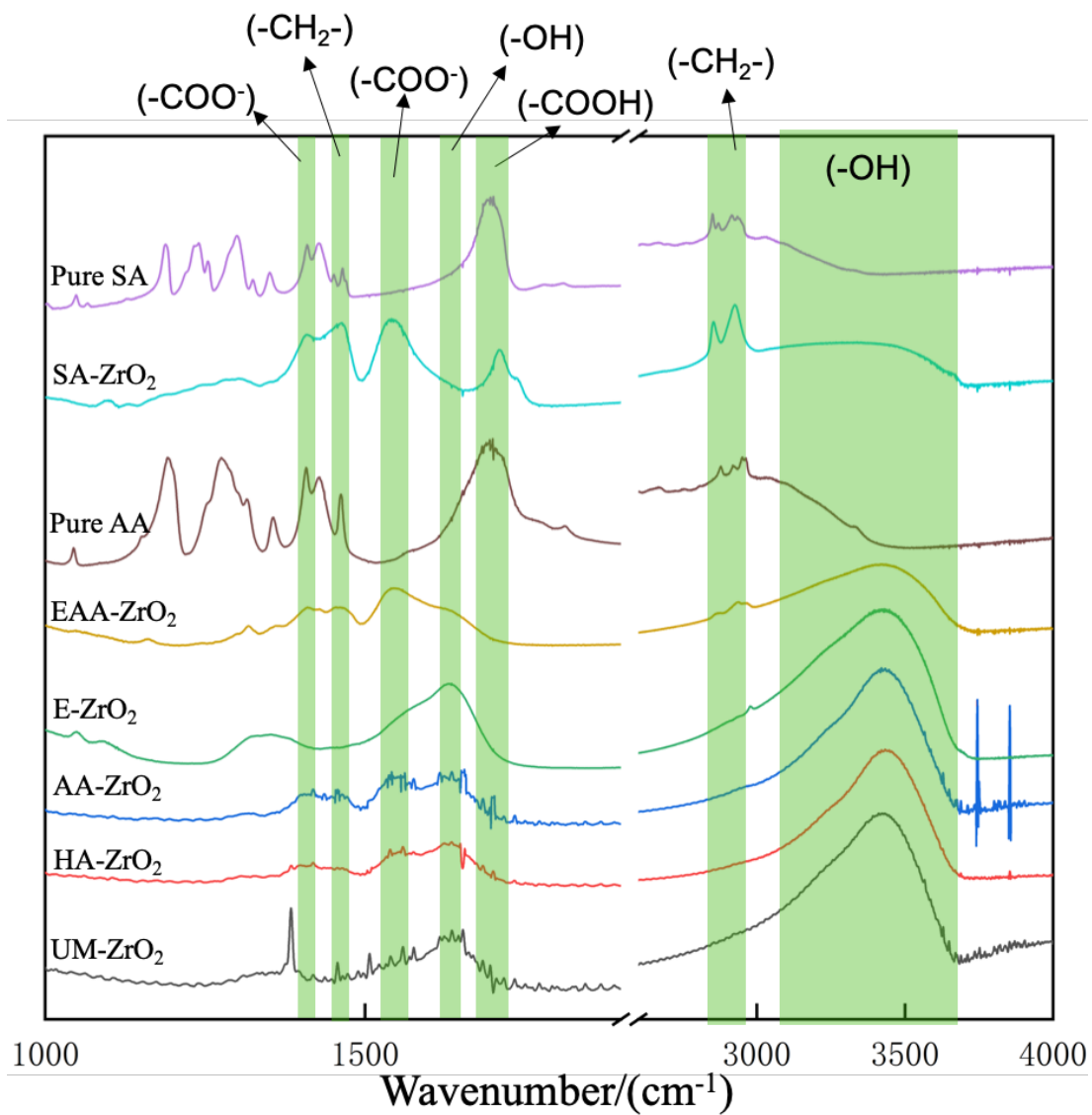
Figure 3.13 FTIR spectra (concentration of modifiers is 0.002 mol/L)

Table 3.1 Size distribution and organic modification results

	Sample Name	Size /(nm)		Modification (mmol/g ZrO$_2$)	Total mass loss (g/g ZrO$_2$)	Modifier ratio of mass loss (g modifier/g mass loss)
		XRD	TEM			
1	UM-ZrO$_2$	5.5	7.5±2.3	-	7.96 %	-
2	002HA-ZrO$_2$	5.7	6.9±2.2	19.6	7.81 %	29.2 %
3	006HA-ZrO$_2$	6.1	7.5±2.2	17.9	6.83 %	30.4 %
4	002AA-ZrO$_2$	5.9	6.8±3.1	25.8	9.32 %	40.5 %
5	006AA-ZrO$_2$	5.2	7.4±2.9	27.6	9.46 %	42.6 %
6	E-ZrO$_2$	5.1	7.8±3.2	-	6.01 %	-
7	002SA-ZrO$_2$	5.5	6.3±2.5	55.3	13.98 %	80.0%
8	006SA-ZrO$_2$	4.9	6.2±2.8	62.7	17.54 %	72.3 %
9	EAA-ZrO$_2$	5.1	7.1±3.3	21.8	5.70 %	55.8%
10	DA-ZrO$_2$	7.8	-	22.4	54.63 %	0.7%

Chapter 4 Summary and Conclusion

4.1 Summary

This study synthesized the ZrO_2 nanoparticles modified by carboxylic acids in supercritical flow reactors. Using short chain (6 C) and long chain (10 C) acid with one or two carboxyl groups as modifiers, ZrO_2 nanoparticles has no remarkable change on size or appearance but changes on crystalline phase can be observed. SA and DA have obvious effect on the stabilization of tetragonal phase. HA and AA, have less selective on tetragonal ZrO_2 but selective on monoclinic as the same as the unmodified ZrO_2. The FTIR also indicate the AA combined particles both two -COOH but SA modified ZrO_2 exists plenty of free -COOH.

4.2 Conclusion and prospect

Overall, the carboxylic acid has no obvious effect on the ZrO_2 nanoparticles morphology but the modified ZrO_2 phase have tetragonal-oriented. And this is considerable to use longer chain acid as modifiers for getting more tetragonal phases. For the modification, di-acids might combine ZrO_2 particles more easily due to two -COOH leading to more chances to contact the particles.

Versatile types of carboxylic acids offer the possibility to modify the nanoparticles in supercritical water. In this study, four chain carboxylic acid as modifiers exhibited their different effect on zirconia. Compared to chain acids containing two carboxyl groups, whether organic acids containing other functional groups have other effects deserves further investigation, such as amino groups, double bonds, and so on. It is worth to explore how these functional groups will affect the modification process and how they affect the growth process of nanoparticles. In addition, in this experiment, the addition of ethanol also showed an obvious effect on the crystal phase selection of zirconia nanoparticles. If the content of ethanol is increased, it is worth to explore that whether it has the potential to improve the selectivity of tetragonal zirconia and what

will happen to the carboxylic acid modification. Not only a variety of modifiers are worth to used, but the reaction condition, like pressure, temperature and residence time also need further discussion. Actually, there is still a long way to go on development of nanoparticle surface modification.

Literature Cited

[1] C. Kagan, C. Murray. *Nat. Nanotechnol.*, 10:1013−1026(2015).

[2] J. Darr, J. Zhang, N. Makwana, *Chem. Reviews*, 117:11125-11238(2017).

[3] T. Harata, *Environ. Syst. Thesis,* 1:1-116(2018).

[4] A. Yoko, G. Seong, T. Tomai, *J. KONA Powder and Particle*, 37:28-41(2020).

[5] N. Thanh, N. Maclean, S. Mahiddine, *Chem. Reviews*, 114:7610-7630(2014).

[6] W. Wagner., A. Pruß, *J. Phys. & Chem. Reference Data*, 31:387−535(2002).

[7] J. Kestin, J. Sengers, B. K., *J. Phys.& Chem. Reference Data*, 13:175-183(1984).

[8] T. Adschiri, K. Kanazawa, K. Arai et al., *J. American. Ceramic Society*, 75:1019-1022(1992).

[9] T. Adschiri, K. Byrappa, *Nanohybridization of Organic-Inorganic Material*, p:247-280(2009).

[10] M. Yoshimura, K. Byrappa, *J. Mater. Sci.*, 43:2085-2103(2008).

[11] N. Makwana, C. Tighe, R. Gruar, *Mater. Sci. Semicond. Process.*, 42:131-137(2016).

[12] N. Aoki, A. Sato, H. Sasaki, *J. Supercritical Fluids*, 110:161-166(2016).

[13] T. Fuji, S. Kawasaki, A. Suzuki, *Cryst. Growth and Design*, 16:1996-2001(2016).

[14] M. Taguchi, N. Yamamoto, D. Hojo, *RSC Adv.*, 4:49605-49613(2014).

[15] D. Rangappa, S. Ohara, T. Naka, *J. Mater. Chem.*, 17:4426-4429(2007).

[16] S. Pujari, L. Scheres, A. Marcells et al., *Angew. Chem. Int. Ed.*, 53:6322-6356(2014).

[17] S. Takami, S. Ohara, T. Adschiri, *Dalton Trans.*, 40:5442-5446(2008).

[18] E. C. Subbarao, H. Maiti, K. Srlvastava, *Phys. Status Solidi A*, 21(1975).

[19] N. Wu, T. Wu, I. Rusakova, *J. Mater. Res.*, 16(2001).

[20] Y. Hakuta, T. Ohashi, H. Hayashi et al., *J. Mater. Res.*, 19:2230-2234(2004).

[21] R. Garvie, *J. Phys. Chem.*, 82:218-224(1978).

[22] X. Bokhimi, A. Morales, O. Novaro, *Nanostruct. Mater.*, 12:593-596(1999).

[23] J. Becker, P. Hald, M. Bremholm et al., *ACS Nano.,* 2:1058−1068(2008).

[24] M. Taguchi, S. Takami, T. Adschiri et al., *CrystEngComm.,* 14:2132–2138(2012).

[25] T. Harata, *J. Utokyo,* 1-116(2018)

[26] A. Auxéméry, G. Philippot, *J. Mater. Chem.*, 32:8169-8181(2020).

Acknowledgments